J. Am. Soc. Mass Spectrom. (2016) 27:73–82
DOI: 10.1007/s13361-015-1239-2

RESEARCH ARTICLE

New Insights into Active Site Conformation Dynamics of *E. coli* PNP Revealed by Combined H/D Exchange Approach and Molecular Dynamics Simulations

Saša Kazazić,[1] Branimir Bertoša,[2] Marija Luić,[1] Goran Mikleušević,[1] Krzysztof Tarnowski,[3] Michal Dadlez,[3] Marta Narczyk,[4] Agnieszka Bzowska[4]

[1]Division of Physical Chemistry, Ruđer Bošković Institute, Zagreb, Croatia
[2]Division of Physical Chemistry, Faculty of Science at University of Zagreb, Zagreb, Croatia
[3]Institute of Biochemistry and Biophysics Department, Polish Academy of Science, Warsaw, Poland
[4]Division of Biophysics, Institute of Experimental Physics, University of Warsaw, Warsaw, Poland

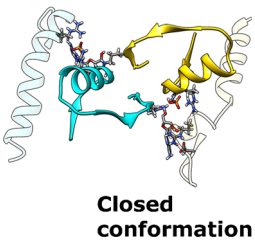

Abstract. The biologically active form of purine nucleoside phosphorylase (PNP) from *Escherichia coli* (EC 2.4.2.1) is a homohexamer unit, assembled as a trimer of dimers. Upon binding of phosphate, neighboring monomers adopt different active site conformations, described as open and closed. To get insight into the functions of the two distinctive active site conformations, virtually inactive Arg24Ala mutant is complexed with phosphate; all active sites are found to be in the open conformation. To understand how the sites of neighboring monomers communicate with each other, we have combined H/D exchange (H/DX) experiments with molecular dynamics (MD) simulations. Both methods point to the mobility of the enzyme, associated with a few flexible regions situated at the surface and within the dimer interface. Although H/DX provides an average extent of deuterium uptake for all six hexamer active sites, it was able to indicate the dynamic mechanism of cross-talk between monomers, allostery. Using this technique, it was found that phosphate binding to the wild type (WT) causes arrest of the molecular motion in backbone fragments that are flexible in a ligand-free state. This was not the case for the Arg24Ala mutant. Upon nucleoside substrate/inhibitor binding, some release of the phosphate-induced arrest is observed for the WT, whereas the opposite effects occur for the Arg24Ala mutant. MD simulations confirmed that phosphate is bound tightly in the closed active sites of the WT; conversely, in the open conformation of the active site of the WT phosphate is bound loosely moving towards the exit of the active site. In Arg24Ala mutant binary complex P_i is bound loosely, too.

Keywords : Allostery, Negative cooperativity, Phosphate binding site, Purine metabolism, Purine nucleoside phosphorylase

Abbreviations PNP Purine nucleoside phosphorylase; FA Formycin A; P_i Phosphate ion; H/DX MS Hydrogen/Deuterium Exchange Mass Spectrometry; MD Molecular Dynamics

Received: 12 April 2015/Revised: 24 July 2015/Accepted: 26 July 2015/Published Online: 3 September 2015

Introduction

The allosteric regulation of the protein function is a fundamental phenomenon important for numerous cellular processes including, among others, metabolic control, receptor and channels functions, ligand transport, and mobility [1–3]. Allostery is a manifestation of residue communication between remote parts in a protein that mediates molecular controls. Chemically and physically induced motions for functions and molecular interactions range from residue side chain flipping, domain rearrangement, to global motions of monomers that are committed to form complexes. The time and spatial scales of these complicated motions range from picoseconds to seconds and from nanometers to micrometers requiring a variety of experimental, e.g., spectroscopic and simulation approaches

Electronic supplementary material The online version of this article (doi:10.1007/s13361-015-1239-2) contains supplementary material, which is available to authorized users.

Correspondence to: Saša Kazazić; *e-mail:* kazazic@irb.hr, Branimir Bertoša; *e-mail:* bbertosa@chem.pmf.hr

to get insight into relations between protein dynamics and biological functions [4].The thoroughly studied example is hemoglobin allostery with positive cooperativity between subunits [5, 6]. The versatile approaches used for these studies involve time-resolved protein crystallography based on recently introduced X-ray free electron laser method (XFEL) suitable to resolve dynamics, particularly related to proton transfer through H-bonds, at ultrafast time (femtosecond) scale [7].

It is a challenging problem of molecular biophysics to elucidate how the allosteric signal is transmitted along the protein. Furthermore, it is important to know whether the communication between distinct sites within a protein molecule is the result of displacement of some structural elements of protein or changes in the dynamics and the flexibility of the protein [8–10]. One of the intriguing aspects of this problem seems to be the allosteric regulation in homooligomeric proteins that result in a very strong negative cooperativity accomplished by ligand-induced conformational changes taking place in some but not in all subunits [11–14]. Binding of a ligand to one subunit results in weaker binding of a next ligand molecule to the neighboring subunit(s). A well-known example of such an enzyme is thymidylate synthase (TS), an obligate homodimer, which catalyzes the reductive methylation of deoxyuridine monophosphate (dUMP, substrate) by 5,10-methylenetetrahydrofolate (cofactor) to generate thymidylate (dTMP) and dihydrofolate [15]. The simultaneous occupancy of the cofactor and substrate at one monomer triggers a transition between a free TS open form to a bound TS closed form with C-terminus closing the active-site pocket. This leads to the formation of a covalent bond between the catalytic cysteine and dUMP, but also initiates a cascade of conformational changes that prevent covalent bond formation and cofactor binding at the neighboring monomer, which remains in the open conformation. The crystal structure of TS from *Pneumocystis carinii* ternary complex, with substrate dUMP and a cofactor mimic, identified a direct route of the communication between TS subunits [16]. Several residues, specifically 173-176 and 196-199 at the dimer interface that form a direct connection between the two neighboring active sites, undergo (upon binding of ligands) a strong coordinated movement within a rather rigid dimer interface resulting in marked structural differences between the two subunits. Hence, in the case of TS, the communication pathway between the two active sites is evident in the static picture obtained from X-ray studies.

Similarly, the communication path was identified for some other negatively cooperating homooligomeric enzymes. An example is the bovine prostaglandin endoperoxide H synthase-1 (also known as cyclooxygenase). Cross-talk between monomers within the dimer involves interaction of two mobile loops located at the dimer interface, which change orientation relative to one another upon ligand binding [17]. The mechanism of subunit interactions is also evident from the crystal structure of tryptophanyl-tRNA synthetase II from *Deinococcus radiodurans*; upon binding of tryptophan, the dimer interface region of both subunits shifts towards the occupied site, while the resulting side chain movements and switching H-bonding partners propagate structural changes to the neighboring active site [18].

By contrast, such a path could not be identified from the X-ray structure of *E. coli* homohexameric purine nucleoside phosphorylase (PNP; EC 2.4.2.1). This remarkable enzyme has been the subject of our scientific interest for many years [19–24]. PNPs are versatile catalysts of the reversible phosphorolysis of purine (2′-deoxy)-ribonucleosides [25, 26]:

purine (2′-deoxy)-ribonucleoside + orthophosphate ↔ purine base + (2′-deoxy)-ribose 1-phosphate

Due to their catalytic function and much broader specificity compared with their trimeric human counterpart [26], hexameric PNPs (e.g., from *E. coli*) have been investigated for the efficient synthesis of nucleoside analogues [27] as well as for the activation of pro-drugs in anti-cancer gene therapies [28]. The key role of PNPs in the purine salvage pathways made them also attractive targets for drug design against several pathogens [29–32].

Hexameric *E. coli* PNP, in fact structurally a trimer of dimers, in the ligand-free form is a symmetrical molecule with open active sites [3, 17] (Figure 1b). The monomers within a dimer mutually donate each other the two side chains necessary to complete the active site, His4 and Arg43. Upon binding of the phosphate (as in TS upon binding of the cofactor) and its interaction with Arg24, conformational change takes place but only in one monomer within a dimer. Segmentation of the C-terminal helix H8 occurs, resulting in a partial closing of the entrance to the active site pocket (closed form). This moves Arg217 close to the catalytic Asp204. These changes in one monomer render its neighbor within a dimer incapable of closing the active site pocket; therefore the enzyme molecule becomes a trimer of unsymmetrical dimers. This implies that a mechanism must exist for information transfer from the active site of one monomer to the other. However, no such mechanism could be derived from the *E. coli* PNP crystal structures [20, 21]. The two active sites within a dimer are about 20 Å apart, and the flexible α-helices H8, one of which undergoes a conformational change, point in opposite directions. The interface of subunits forming a dimer buries 32 water molecules that are not connected with the bulk water [20]. An intriguing question is how the information on the conformational changes of one active site is transferred to the neighboring subunit within the dimer. One possible reason is that ligand binding induces only changes in protein dynamics that are not visible in the static, time-averaged picture delivered by X-ray crystal structure. To check this hypothesis, in the project reported here, H/D exchange mass spectrometry (H/DX MS) approach [33] combined with molecular dynamics (MD) simulations [34] were performed. Typically, protein 3D structures obtained by X-ray or NMR are a starting point for computational analysis aimed to obtain structure parameters important for H/DX data interpretation. Different calculation strategies are employed to link protein dynamics with amide H/DX reaction rates by analyzing ensemble representation of the protein structure [35–39]. All-atom molecular dynamics (MD) simulations can be used to probe protein structure flexibility caused by frequent atomic movements [40, 41] but other fluctuations relevant for H/DX occur on a time scale longer than it is currently possible to simulate with average computation resources. Recently,

McAllister and Konermann carried out detailed structure-exchange rate relationship analysis by combining MD simulations and H/DX data and showed that significant fraction of amide hydrogens exist with H/DX protection different than can be predicted by any of the current models proposed to explain particular H/DX pathway [42]. Skinner et al. analyzed a large residue resolved H/DX dataset obtained for protein with known biophysical properties to examine interplay of static and dynamic structural factors and provided detailed view on how they determine measured amide H/DX rates [43, 44]. In the present work, MD simulations were carried out to provide a dynamic view of the protein ground state within a solvent environment for all experimentally investigated protein forms. These structures represent a better comparison basis for the interpretation of the H/DX data than a single static X-ray structure of the ternary complex published earlier [20].

Experiments were done for the wild type *E. coli* PNP and its Arg24Ala mutant, in the ligand-free form, as well as in binary and ternary complexes with the substrate (orthophosphate) and with the noncleavable nucleoside substrate analogue, formycin A (an inhibitor) [45] see Scheme 1.

Materials and Methods

E. coli PNP Sample Preparation

Overexpression of recombinant *E. coli* PNP WT and Arg24Ala mutant was done in *E. coli* strain BL21 (DE3). Enzymes were purified in a two-step procedure using Q-Sepharose FF anion exchange chromatography and gel filtration on Sephacryl S-200 column as previously described [21]. After purification, samples in 20 mM Tris-HCl, pH 7.4 were concentrated to 2.8 mM by ultrafiltration at 4000 g using Vivaspin 2 (10000 MWCO) centrifugal concentrators (Sartorius Stedim Biotech). For a complete differential H/D exchange study, six protein samples were prepared: ligand-free WT and mutant Arg24Ala protein (2 mM), their complexes with a phosphate ion (P_i, 50 mM) and their complexes with a P_i (50 mM) and formycin A (FA, 5 mM). For each of the six samples, 150 μL of protein stock solution was produced by stock sample dilution with 20 mM Tris-HCl, pH 7.4, to a 75 μM PNP concentration. For making a dilution buffer for ligand free samples, particular care was dedicated to avoid contamination with P_i.

Hydrogen/Deuterium Exchange Mass Spectrometry Experiment

Experiments were conducted at room temperature. For each of six stock solutions, data were collected for five different H/D exchange periods (10 s, 1 min, 20 min, 60 min, 240 min) and for three controls (undeuterated sample, in-exchange control, and out-exchange control). Each set of conditions was repeated in triplicate, for a total of 24 individual trials per one stock solution. The experimental steps for one individual trial included the start with 1/10 sample dilution into a deuterated buffer to initiate exchange. Five μL of 75 μM stock solution was added to 45 μL of reaction buffer for each exchange time period. The reaction progress was terminated by transferring 50 μL of reaction solution into a 10 μL of a quench buffer, incubated on ice, causing a rapid decrease of pH to 2.4, and lowering the temperature to ~0°C.

The resulting 60 μL of cold protein solution were further analyzed on a Waters H/DX technology platform [33] as described in Tarnowski et al. [47]. A reproducible peptide list was assembled by using an in-house produced program for HD/X data analysis [48] and the Waters ProteinLynx Global Server (Waters, Milford, MA, USA). Hydrogen/deuterium exchange data were analyzed by the Waters DynamX 2.0 software package, permitting accurate assignment of the deuterium incorporation as described elsewhere [47].

To present a sample flexibility map determined in the H/DX experiment, fractions exchanged were calculated for each peptide at each time period, with the normalization of the observed deuterium uptake to the maximum number of exchangeable amides within a peptide. Five differential comparisons of the H/DX data collected for six samples were carried out according to procedure described elsewhere [49].

Molecular Dynamics Simulations

Analogous to six samples that were studied experimentally, six systems of *E. coli* PNP were built in silico and prepared for MD simulations. Ligand-free systems were produced from 1ECP (PDB code) PNP crystal structure [50], in the apo form with all six sites in the open conformation; all WT and Arg24Ala mutant complexes were built from 1K9S (PDB code) WT PNP crystal structure [20], which has three active sites in open and three in closed conformations. Sulphate ions that are present in this structure were replaced by P_i. Arg24Ala mutant structures were prepared by introducing mutations into these 3D structures. Crystal water molecules found within 3 Å from the protein heavy atoms were retained for simulations. WHAT IF software [51] was used for adding polar hydrogen atoms, while nonpolar hydrogen atoms were added with the *t-leap* module of the AMBER program package [52]. Parameterization of protein atoms was accomplished with the amber ff03 force field [53]. Purine nucleoside and P_i were parameterized using the *antechamber* module of the AMBER program package [52]. The protein was centred in a rectangular parallelepiped box filled with TIP3P water molecules [54]. The systems were neutralized by adding sodium ions [55].

These six systems were energy-minimized and geometry-optimized in five cycles. Each cycle consisted of 1000 steps of a steepest descent algorithm followed by 4000 steps of a conjugated gradient algorithm. In the first three cycles, protein and substrate atoms, protein heavy atoms and substrate atoms, and protein backbone atoms and substrate atoms, respectively, were constrained using a 100 kcal/(mol·Å^2) force constant. In the fourth cycle, the force constant on the protein backbone atoms and substrate atoms was decreased to 50 kcal/(mol·Å^2). Lastly, in the fifth cycle, no constraints were applied.

After geometry optimization, the systems were subjected to 5.5 ns of MD simulations (only the *E. coli* WT PNP ternary

complex was simulated for 4.5 ns). The temperature was linearly increased from 0 to 300 K during the first 250 ps and kept constant (300 K) during the rest of the simulation using the thermostat of Berendsen et al. [56]. During the first 300 ps, protein and substrate atoms were constrained (25 kcal/(mol·Å^2)) and the volume was kept constant. The rest of the simulation was conducted without any constrains on atoms, and the pressure was kept constant (101 325 Pa). The time step was 1 fs. Periodic boundary conditions (PBC) were applied. Particle Mesh Ewald (PME) was used for calculation of electrostatic interactions. The cut-off value for nonbonded interactions was set to 10 Å. The geometry optimization and the first 500 ps of MD simulations were conducted using AMBER software [52], whereas the rest of simulations were conducted with Gromacs [57] using the same parameters as described above. All trajectories were analyzed using the VMD program [58] and Gromacs analyzing tools [57].

Results and Discussion

Mobility of the Wild Type and the Arg24Ala E. coli PNP Hexamer

Dynamics of the *E. coli* PNP hexamer was investigated using H/DX mass spectrometry and molecular dynamics (MD)

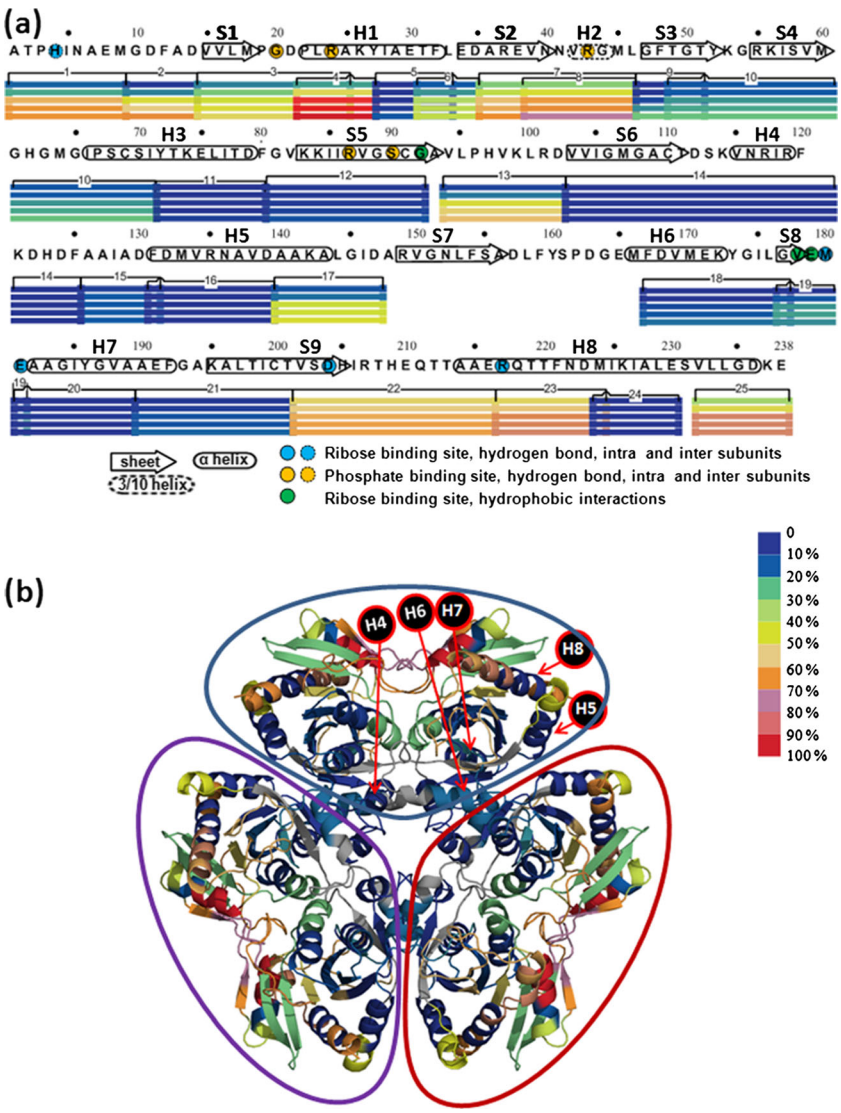

Figure 1. Results of the H/DX MS experiment collected for ligand-free state of the *E. coli* WT PNP protein at pH 7.4 in 20 mM Tris-HCl buffer. Raw data measured for 25 peptides at five time periods (10 s and 1, 20, 60, 240 min) are normalized to the maximum uptake value obtained in full-exchange control experiment, and peptides deuterium uptake percentage, are calculated. For H/DX data visualization, every deuterium uptake percentage value is associated with a corresponding color from stacked color bar. All 3D structures have mapped deuterium uptake percentages which are measured in ligand-free state after 4 h of exchange time. **(a)** Flexibility map obtained by mapping color coded deuterium uptake values for 25 digested peptides at all five time periods to *E. coli* PNP WT protein sequence. Each peptide number is shown below the sequence. Color-coded percentages are presented as stacked horizontal lines. **(b)** Three dimers composing the hexamer (top view, PDB 1K9S) are marked by blue, violet, and red circles, respectively. Highly protected helices, H4, H6, and H7, are located at contact interface between dimers are labeled

simulations. Differences in the protein's mobility with respect to the presence of substrate and introduced Arg24Ala mutation were explored by H/D exchange experiments. In these experiments, a ligand-free WT PNP and Arg24Ala mutant, their binary complexes with phosphate ion (P_i), and their ternary complexes with P_i and nucleoside substrate analogue formycin A, an inhibitor (FA) were studied.

On-line pepsin digestion carried out in this study produced 109 *E. coli* PNP peptides common to all studied complexes of the WT and Arg24Ala mutant. The sequence coverage was 94% with one gap of 18 amino acids from 148 to 166. The collected H/D exchange data were mapped to the protein primary sequence covering the 25 smallest peptides with minimal overlap, thereby preserving the initially obtained 94% sequence coverage (Figure 1a).

Protection against H/D exchange of peptides determined at a longest time period of 4 h are mapped onto *E. coli* PNP WT hexamer tertiary structure (Figure 1b, PDB code 1K9S). It can be noticed that the deuterium incorporation is very low at the interface between dimers (helices H5 and H7) and in the middle of the barrel (helices H4 and H6). After the longest exchange period, the averaged deuterium uptake reaches only 32% of all exchangeable hydrogen atoms within 25 peptides; this points out to a high rigidity of enzyme inner core such as an interface between dimers (Figure 1b, Figures S1 and S2 in Supplementary Information). The regions with a higher H/D exchange reaction rate are localized either on the protein surface or at the interface between monomers within dimers (Figure 1b). Peptides containing His4 [loop, N-terminal peptide 1 (2-10)], Arg24 [H1, peptides 3 (16-26) and 4 (23-28)], and Arg43 [loop, peptides 7 (37-47) and 8 (40-47)], show high deuterium uptake.

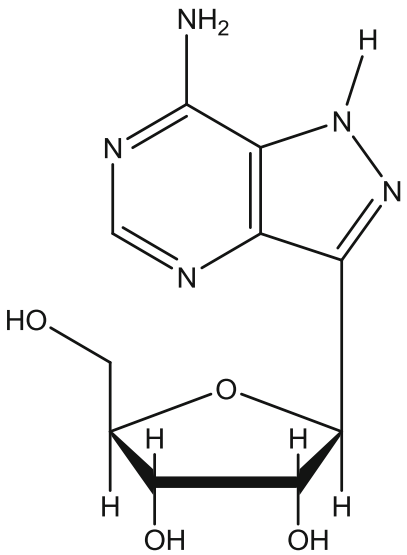

Scheme 1. The structure of formycin A, shown in a preferred tautomeric form (present in 85% in solution) [46]

Comparing the flexibility map of a ligand-free state between WT (Figure 1a) and Arg24Ala mutant (not shown) demonstrate no significant differences. This indicates that the backbone dynamic behavior of ligand-free *E. coli* PNP is unaffected by this mutation. The same conclusion is supported by MD simulations (Figures S1 C, and S2, A and B in Supplementary Information).

On the other hand, significant differences in backbone fluctuations between WT and Arg24Ala were noticed during the MD simulations of their binary and ternary complexes (Figure S1, G–I in Supplementary Information). The largest difference is found in the fluctuation of the segment consisting of residues 212 to 222. This is the part of the H8 helix that is segmented, partly blocking the entrance to the closed active site (Figure S2, C–F in Supplementary Information). However, in the open active site conformations the helix H8 remains straight.

Phosphate Binding is Affected by Arg24Ala Mutation and Active Site Conformation

H/DX MS experiments and MD simulations clearly show differences in P_i binding between the WT and Arg24Ala mutant. Furthermore, simulations also point to the importance of active site conformation for productive P_i binding.

In the closed active site of the *E. coli* WT PNP binary complex, P_i is firmly bound during the whole simulation, making preserved H-bonds with side chains of Arg24, Arg87, Ser90, and Arg43 from the neighboring monomer, and backbone amides of Gly20 and Ser90 (Figure 2c, d, Figure 4, Figure S3 in Supplementary Information). Occasionally, it also makes H-bonds with backbone amide hydrogen of Asp21 and electrostatic interactions with the sodium ion that enters the active site from the solute during the simulation. Measurements of the radius of gyration of the active site during the MD simulations, confirm stability of the closed active site (Figure S7 in Supplementary Information).

By contrast, in the open active sites, the P_i is not stably bound, changing its initial position, getting closer to the exit of the active site in the ns-time scale of simulations (Figure 2c, d, Figure 4); H-bonds with the side chains of Arg24, Ser90, and Arg217, and occasionally with the Arg43 side chain from the neighboring monomer, were observed (Figure 2c, d, Figure S4 in Supplementary Information). In the closed active site, which is more compact, P_i is anchored by strong H-bonds to Arg87, while in the open active site this interaction is lost. The movement of the P_i during the MD simulations is followed by the increase of the radius of gyration of the active site pointing out to the more spatial active site (Figure S7 in Supplementary Information).

In the case of the Arg24Ala PNP binary complex, the P_i is loosely bound in both open and closed active sites during the simulations. During simulations, closed active sites become more open (as supported by the increasing value of the radii of gyration, Figure S7 in Supplementary Information).

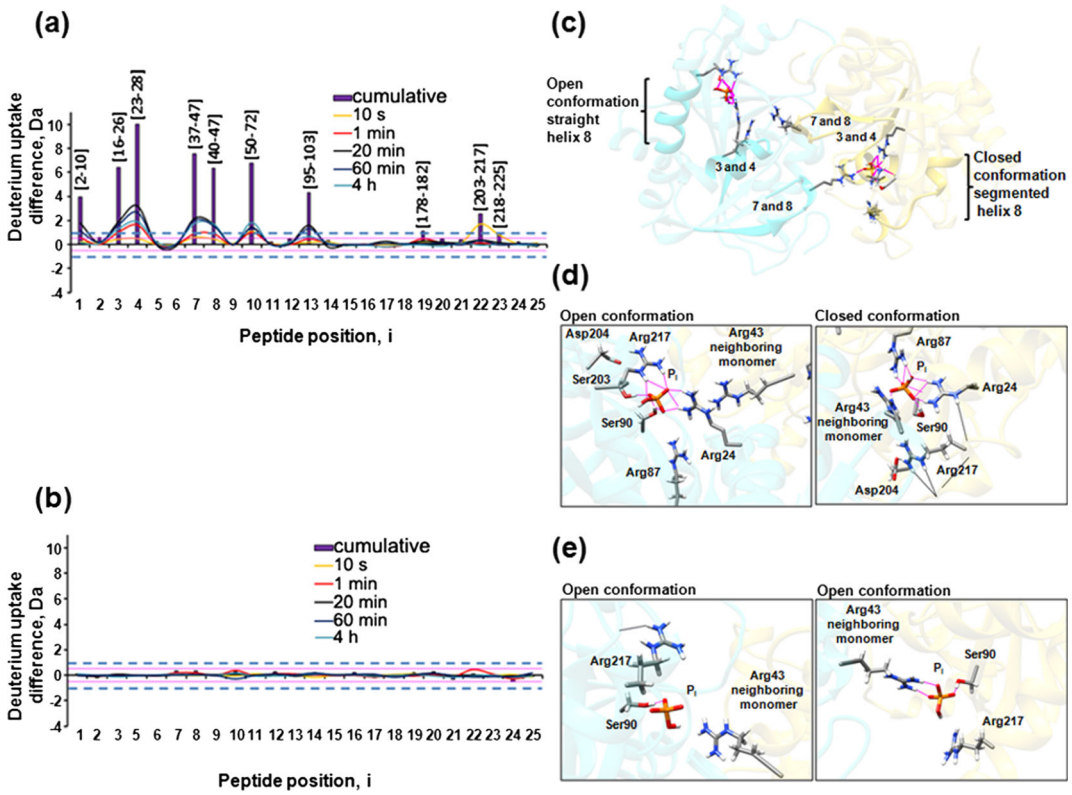

Figure 2. Differential H/DX data for the ligand-free versus binary complex with phosphate and their MD structures after 5 ns simulations. H/D data differences are presented by orange, red, black, light-blue, and blue traces, which correspond to the exchange difference between protein states observed for each peptide at 10 s, 1, 20, 60, and 240 min deuterium incubation time points; red dotted lines represent significance threshold limit of ±0.3 Da for each time period value. Cumulative value is a sum of all deuterium uptake differences observed at each time period of a particular peptide and is plotted as a vertical bar, dashed blue lines denote significance threshold limit of ±0.9 Da for those values. Positive sign of the difference value denotes less deuterium uptake for binary complex than for the ligand-free protein and vice versa. H/D data difference plot comparing ligand-free versus binary complex for: **(a)** *E. coli* PNP WT, **(b)** Arg24Ala mutant *E. coli* PNP. 3D structures are obtained after 5 ns of MD simulation. **(c)** Catalytic dimer of *E. coli* PNP WT/P_i representing interface between monomers with the open (straight H8 helix) and closed (segmented H8 helix) active site. Peptides with largest change in deuterium uptake upon P_i binding are mapped to 3D structure and are labeled by their number. Phosphate ion (orange and red) is placed in active site of both monomers, and its H-bonds are shown. **(d)** Changes of H-bonds in the open and closed active sites are shown (preserved ones are in magenta). Within active site in open conformation, P_i forms H-bonds with Ser90, Arg24 (fragments 3 and 4) and Arg217 making this residue catalytically inactive. Hydrogen bond to Arg43 (fragments 7 and 8) occurs occasionally, whereas bond to Arg87 is entirely lost. Within active site in closed conformation, P_i establishes H-bonds with Ser90, Arg24 (fragments 3 and 4), Arg87, and Arg43 (fragments 7 and 8) from neighboring monomer. Arg217, which is the important residue for catalytic activity, is H-bonded (black line) with Asp204 and Arg24 making helix H8 segmented. **(e)** *E. coli* PNP Arg24Ala mutant with open active sites conformation having disordered P_i with switching H-bond among amino acid residues

In all six active sites, phosphate anions are somewhat disordered; however, their good proton acceptor properties make them accessible for H-bond interactions with side chains of Arg43 (from the neighboring monomer), Ser90 and Arg217 (Figure 2c, e, Figure 4, Figure S5 in Supplementary Information). The lack of positively charged Arg24, due to mutation, cancels a strong H-bond to P_i. Thus, the presence of Arg24 is crucial for productive P_i binding in closed active sites, which stabilizes the closed active site conformation. This is in agreement with H/DX experiments (see Figure 2b).

H/DX comparative analysis for 25 selected peptides produced a set of differences between deuterium uptake values of ligand-free and binary complex for WT PNP and its Arg24Ala mutant presented in Figure 2a and b, respectively. In this analysis, differences in protection are identified by subtracting normalized triplicate-averaged deuterium uptakes measured for the binary complex from those measured for the ligand-free form. A positive difference indicates slower H/D exchange for the binary complex [49].

The H/DX method cannot distinguish conformational changes induced by P_i binding to a single active site of the PNP hexamer because measurements provide values averaged over all PNP conformation states present in solution. Nevertheless, on average, significant differences can be noted comparing deuterium uptake values for 25 peptides in the ligand-free WT PNP and binary WT PNP/P_i complex.

The arrest of the molecular motion is observed in almost all peptides identified as backbone-flexible in the ligand-free state. The most pronounced decrease in backbone H/D exchange was observed for peptides 3 (16-26) and 4 (23-28), both containing Arg24, and peptides 7 (37-47) and 8 (40-47), both containing Arg43 from a neighboring monomer subunit (Figure 2a, c). Other regions located close to the active site [peptides 10 (50-72), 13 (95-103), and 19 (178-182)], and peptides 1 (2-10) and 10 (50-72) from adjacent subunit are under the influence of the P_i. This suggests that information of phosphate binding at the active site of one monomer is transmitted to the neighboring active site (separated by about 20 Å) by decreasing molecular motion of the protein. The communication between monomers within the catalytic dimer can be understood as allostery. However, fine-tuning of the communication between the two active sites can be established by time-resolved X-ray free electron laser crystallography [59].

For the two peptides, 22 (203-217) and 23 (218-225), which are part of H8 helix becoming segmented in a closed active site conformation, the presence of the bound P_i in WT influences just the fast exchanging unprotected amide hydrogens (Figure 2a).

In contrast to the WT PNP, almost inactive Arg24Ala mutant does not show any of the slow-down effects when complexed with phosphate (compare Figure 2b with 2a). This finding is in agreement with the observation that all active sites in the Arg24Ala mutant complexed with P_i are open with loosely bound phosphate anion. These remarkable difference even made us suspicious about the binding of the P_i by the Arg24Ala mutant, although it was previously shown by measuring effects of the ligand on the thermal stability of the enzyme [21]. Moreover, binding must take place since the mutant exhibits activity, albeit small (0.2%-0.6% that of the WT) versus natural substrates, and good activity versus 7-methylguanosine (30% that of the WT) [21]. Therefore, we decided to confirm the binding using other approaches, namely

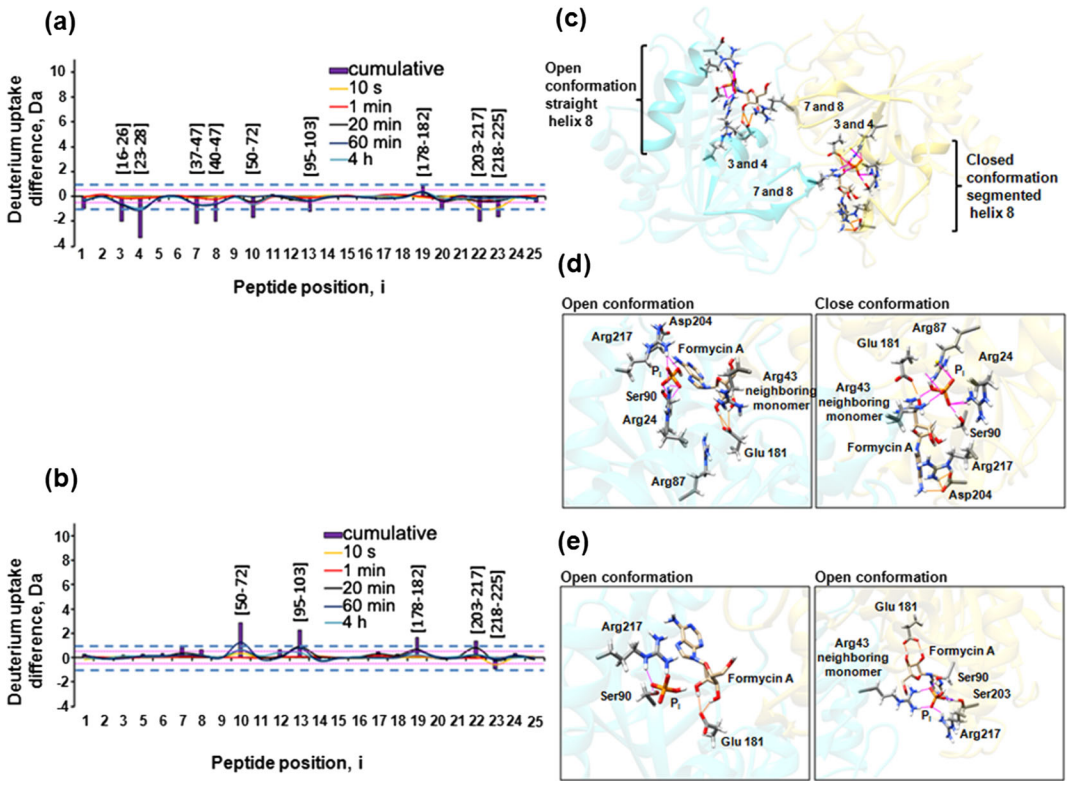

Figure 3. Differential H/DX data for the binary complex with phosphate versus ternary complex with phosphate and formycin A and their MD structures after 5 ns simulations. H/D data difference plot comparing binary versus ternary complex for (**a**) *E. coli* PNP WT, (**b**) Arg24Ala mutant *E. coli* PNP. Legend for H/DX data corresponds to one given in Figure 2. (**c**) Catalytic dimer of *E. coli* PNP ternary complex representing interface between monomers with the open (straight H8 helix) and closed (segmented H8 helix) active site. Peptides with largest change in deuterium uptake upon P_i binding are mapped to 3D structure and are labeled by their number. Phosphate ion (orange and red) and formycin A (brown and blue) are in the active sites. (**d**) In the open conformation of the *E. coli* PNP ternary complex active site P_i forms preserved H-bonds with Arg217, Arg24, and Ser90, whereas interaction to Arg43 from neighboring monomer occurs occasionally; H-bond to Arg87 is lost. In the closed active site conformation, all ligands are positioned properly for the catalytic activity (protonation of the purine base N7 position). (**e**) Ternary complex of the *E. coli* PNP Arg24Ala mutant like in binary complex reveals only open active sites with disordered P_i switching H-bond among amino acid residues as illustrated in two panels

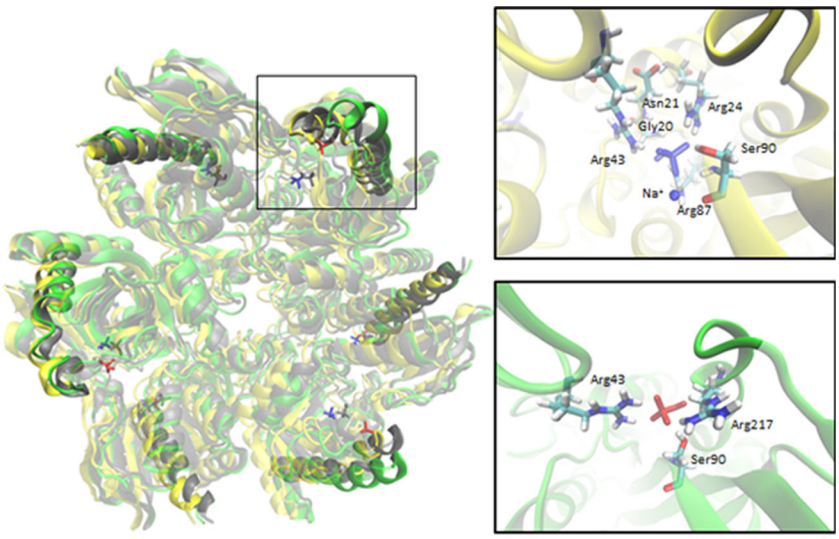

Figure 4. Superimposed structures of *E. coli* PNP binary complexes with P_i. Starting structure (grey), structures obtained after 5 ns of simulation of *E. coli* PNP WT binary complex (yellow) and Arg24Ala mutant binary complex (green). H8 helix is posted in all three structures. Phosphate ion is shown in stick representation and colored orange – starting structure, blue – *E. coli* PNP WT binary complex, red – Arg24Ala mutant binary complex. Phosphate binding site for *E. coli* PNP WT binary complex (upper right square) and Arg24Ala mutant binary complex (lower right square) for one monomer with closed active site conformation in the starting structure are enlarged

near UV-CD spectroscopy and thermophoresis. Both methods confirmed that P_i interacts with the Arg24Ala mutant (A. Bzowska, M. Narczyk and A. Oksiejuk, unpublished data).

Absence of any conformational change upon P_i binding to Arg24Ala mutant emphasizes the role of the Arg24 as a crucial residue for P_i ligation in a stable, long-existing form (in the time scale of catalytic events). The absence of Arg24 disables productive binding of P_i. Thus, the interaction of P_i with this particular residue regulates the overall backbone motion within hexamer, important in transmission of the information about binding from one active site to the neighboring one within the dimer, and can be seen as allostery process.

Forming a binary complex with P_i is only the first step in the catalysis; the next one is nucleoside binding. The WT binary complex becomes slightly relaxed upon binding of formycin A and forming a ternary complex; it occurs in all structure regions where P_i binding causes significant dynamic arrest (Figure 3a). By contrast, ternary complex of the Arg24Ala mutant exhibits slower deuterium exchange kinetics in structure regions covered by peptides 13, 19, and 22 containing amino acids that are known from crystallographic structure that make H-bonds with the ribose part of the ligand (Figure 3b). Opposite deuterium uptake differences, positive for the Arg24Ala mutant (Figure 3b, exchange decreased upon FA binding) and negative for WT (Figure 3a, exchange increased upon FA binding) indicate important differences in dynamics and flexibility of active site within binary complex of these two enzyme forms (Figure 4).

MD simulations of *E. coli* PNP ternary complexes show that Arg24Ala mutation affects only P_i binding; it does not affect nucleoside binding (Figure 3e).

During these simulations, nucleoside remains bound in a similar position as in the starting structure in all active sites of

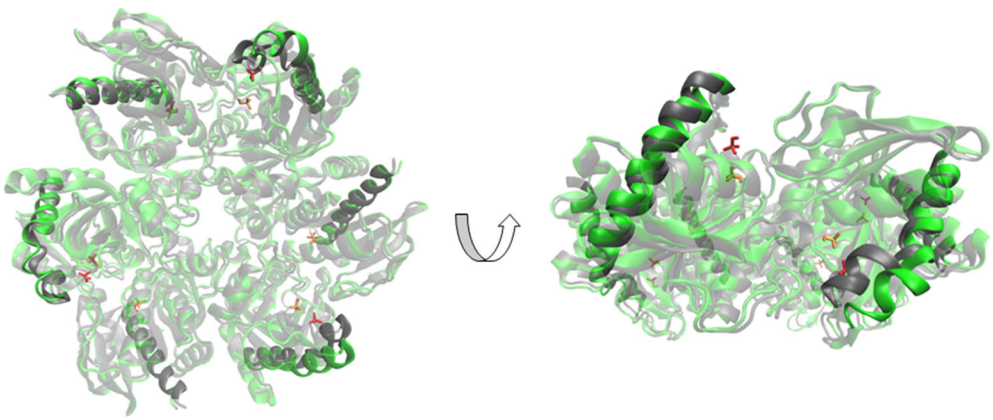

Figure 5. Superimposed structures of Arg24Ala mutant binary complexes with phosphate from two angles. Starting structure (grey) and structure obtained after 5 ns of simulation (green). H8 helix is posted in both structures. Phosphate ion is shown in stick representation and colored orange – starting structure, red – obtained after 5 ns of simulation

WT PNP and its Arg24Ala mutant (Figure 3c, Figure S6 in Supplementary Information). On the other hand, the stability of P_i binding in ternary complexes is the same as previously described for the binary complexes: strongly affected by the conformation of the active site (open or closed) and the Arg24Ala mutation (Figure 3d, e). Stable P_i binding in ternary complexes is retained, similarly as in binary complexes, only in the closed active sites of the WT PNP (Figure 3d).

Phosphate movement during the simulation induces conformational change of the closed active site into the open active site (Figure 3d, e, Figure 5). This conformational change causes the observed increase of fluctuations of the segmented part of H8 helices (residues 212 to 222) during the simulations of Arg24Ala binary and ternary complexes. Such conformational change did not occur during the simulation of WT binary and ternary complexes, in which initially closed active sites retain the closed conformation during the whole simulation.

Conclusion

E. coli PNP is a homohexamer assembled as a trimer of dimers. Neighboring monomers within a dimer, upon binding of phosphate, adopt different, open and closed, active site conformations accompanied by switching H-bonds between phosphate anions and charged amino acid residues Arg24, Arg43, and Arg87, indicating allosteric communication between active sites. However, the static, time-averaged X-ray crystal structure cannot reveal steps in communication between neighboring active sites. Thus, in this study, H/DX mass spectrometry assisted by molecular dynamics simulations is employed. H/DX exchange clearly recognizes the mobile peptides within the enzyme whereas the differential H/DX data reveal changes in their mobility under the influence of P_i binding being related to allostery phenomenon. The impact of P_i binding on the closed and open active sites in the enzyme cannot be seen directly from mass spectrometry measurements but can be visualized in particular enzyme segments by molecular dynamics simulations (Figure 2d, e, Figure 3d, e). Both approaches revealed *E. coli* PNP enzyme to be a protein of moderate mobility with a few flexible regions located either at the protein surface or at the interface between monomers within a dimer. However, the interface between the dimers is recognized as the rigid sections of the protein.

Furthermore, both methods indicated an importance of Arg24 residue for productive P_i binding, which stabilizes the active sites in the closed conformations, necessary for efficient catalysis. Although P_i is surrounded by several positively charged amino acid residues from the active site, a single mutation of Arg24 to Ala changes significantly P_i binding as revealed by experiments and MD simulations. Negative, doubly charged phosphate anion rearranges, upon binding, H-bonds, and attracts positively charged residues affecting dynamics of protein backbone. In this context, the use of Arg24Ala mutant in this work confirmed previous knowledge [19–24] on the key role of Arg24 in the PNP catalysis. Arg24Ala mutant P_i complex does not show any of the slow-down effects noticed within WT/P_i binary complex. Therefore, H/DX experiments suggest that in the case of Arg24Ala mutant P_i binds in a nonproductive manner and cannot stabilize the closed active site conformation. This result is supported by MD simulations. Computational results also showed that P_i is productively bound only in the closed active sites of the WT PNP enzyme.

Acknowledgments

The authors gratefully acknowledge Dr. Biserka Kojić-Prodić for numerous discussions and enormous help in clarifying some parts of the manuscript. The authors are indebted to Mrs. Aleksandra Oksiejuk for near UV-CD experiments, Mrs. Maria Winiewska and Professor Jaroslaw Poznanski from the Institute of Biochemistry and Biophysics (Warsaw) for thermophoresis experiment, and to Dr. Beata Wielgus-Kutrowska for helpful discussion regarding communication of subunits in homooligomeric enzymes. This work was supported by the Polish Ministry of Science and Higher Education grant N N301 044939, Centre of Preclinical Research and Technology grant POIG.02.02.00-14-024/08-00, and NanoFun grant POIGT.02.02.00-00-025/09, by the Croatian Science Foundation under the project 7423 and by European Union's Seventh Framework Programme for Research and Technological Development under grant agreement no. 316289 - InnoMol, FP7-REGPOT-2012-2013-1.

References

1. Peracchi, A., Mozzarelli, A.: Exploring and exploiting allostery: models, evolution, and drug targeting. Biochim. Biophys. Acta – Proteins Proteomics **1814**, 922–933 (2011)
2. Changeux, J.-P.: Fifty years of allosteric interactions: the twists and turns of the models. Nat. Rev. Mol. Cell Biol. **14**, 819–829 (2013)
3. Cornish-Bowden, A.: Understanding allosteric and cooperative interactions in enzymes. FEBS J. **281**, 621–632 (2014)
4. Motlagh, H.N., Wrabl, J.O., Li, J., Hilser, V.J.: The ensemble nature of allostery. Nature **508**, 331–339 (2014)
5. Brunori, M.: Variations on the theme: allosteric control in hemoglobin. FEBS J. **281**, 633–643 (2014)
6. Yuan, Y., Tam, M.F., Simplaceanu, V., Ho, C.: New look at hemoglobin allostery. Chem. Rev. **115**, 1702–1724 (2015)
7. Levantino, M., Schirò, G., Lemke, H.T., Cottone, G., Glownia, J.M., Zhu, D., Chollet, M., Ihee, H., Cupane, A.: Cammarata M: Ultrafast myoglobin structural dynamics observed with an X-ray free-electron laser. Nat. Commun. **6**, 1–6 (2015)
8. Kern, D., Zuiderweg, E.R.P.: The role of dynamics in allosteric regulation. Curr. Opin. Struct. Biol. **13**, 748–757 (2003)
9. Goodey, N.M., Benkovic, S.J.: Allosteric regulation and catalysis emerge via a common route. Nat. Chem. Biol. **4**, 474–482 (2008)
10. Laskowski, R.A., Gerick, F., Thornton, J.M.: The structural basis of allosteric regulation in proteins. FEBS Lett. **583**, 1692–1698 (2009)
11. Koshland Jr., D.E.: The structural basis of negative cooperativity: receptors and enzymes. Curr. Opin. Struct. Biol. **6**, 757–761 (1996)
12. Stevens, S.Y., Sanker, S., Kent, C., Zuiderweg, E.R.P.: Delineation of the allosteric mechanism of a cytidylyltransferase exhibiting negative cooperativity. Nat. Struct. Mol. Biol. **8**, 947–952 (2001)
13. Nørager, S., Arent, S., Björnberg, O., Ottosen, M., Leggio, L.L., Jensen, K.F., Larsen, S.: *Lactococcus lactis* dihydroorotate dehydrogenase A mutants reveal important facets of the enzymatic function. J. Biol. Chem. **278**, 28812–28822 (2003)

14. Cornish-Bowden, A.: The physiological significance of negative cooperativity revisited. J. Theor. Biol. **319**, 144–147 (2013)
15. Carreras, C.W., Santi, D.V.: The Catalytic mechanism and structure of thymidylate synthase. Annu. Rev. Biochem. **64**, 721–762 (1995)
16. Anderson, A.C., O'Neil, R.H., DeLano, W.L., Stroud, R.M.: The structural mechanism for half-the-sites reactivity in an enzyme, thymidylate synthase, involves a relay of changes between subunits. Biochemistry **38**, 13829–13836 (1999)
17. Sidhu, R.S., Lee, J.Y., Yuan, C., Smith, W.L.: Comparison of cyclooxygenase-1 crystal structures: cross-talk between monomers comprising cyclooxygenase-1 homodimers. Biochemistry **49**, 7069–7079 (2010)
18. Buddha, M.R., Crane, B.R.: Structures of tryptophanyl-tRNA synthetase II from *Deinococcus radiodurans* bound to ATP and tryptophan: insight into subunit cooperativity and domain motions linked to catalysis. J. Biol. Chem. **280**, 31965–31973 (2005)
19. Koellner, G., Luić, M., Shugar, D., Saenger, W., Bzowska, A.: Crystal structure of the ternary complex of *E. coli* purine nucleoside phosphorylase with formycin B, a structural analogue of the substrate inosine, and phosphate (sulphate) at 2.1 Å resolution. J. Mol. Biol. **280**, 153–166 (1998)
20. Koellner, G., Bzowska, A., Wielgus-Kutrowska, B., Luić, M., Steiner, T., Saenger, W., St piński, J.: Open and closed conformation of the E. coli purine nucleoside phosphorylase active center and implications for the catalytic mechanism. J. Mol. Biol. **315**, 351–371 (2002)
21. Mikleušević, G., Štefanić, Z., Narczyk, M., Wielgus-Kutrowska, B., Bzowska, A., Luić, M.: Validation of the catalytic mechanism of *Escherichia coli* purine nucleoside phosphorylase by structural and kinetic studies. Biochimie **93**, 1610–1622 (2011)
22. Štefanić, Z., Mikleušević, G., Narczyk, M., Wielgus-Kutrowska, B., Bzowska, A., Luić, M.: Still a long way to fully understanding the molecular mechanism of *Escherichia coli* purine nucleoside phosphorylase. Croat. Chem. Acta **86**, 117–127 (2013)
23. Štefanić, Z., Narczyk, M., Mikleušević, G., Wielgus-Kutrowska, B., Bzowska, A., Luić, M.: New phosphate binding sites in the crystal structure of *Escherichia coli* purine nucleoside phosphorylase complexed with phosphate and formycin A. FEBS Lett. **586**, 967–971 (2012)
24. Bertoša, B., Mikleušević, G., Wielgus-Kutrowska, B., Narczyk, M., Hajnić, M., Leščić Ašler, I., Tomić, S., Luić, M., Bzowska, A.: Homooligomerization is needed for stability: a molecular modelling and solution study of *Escherichia coli* purine nucleoside phosphorylase. FEBS J. **281**, 1860–1871 (2014)
25. Pugmire, M.J., Ealick, S.E.: Structural analyses reveal two distinct families of nucleoside phosphorylases. Biochem. J. **361**, 1–25 (2002)
26. Bzowska, A., Kulikowska, E., Shugar, D.: Purine nucleoside phosphorylases: properties, functions, and clinical aspects. Pharmacol. Ther **88**, 349–425 (2000)
27. Condezo, L.A., Fernandez-Lucas, J., Garcia-Burgos, C.A., Alcántara, A.R., Sinisterra, J.V.: In: Patel, R.N. (ed.) Enzymatic Synthesis of Modified Nucleosides. CRC Press, Boca Raton (2006)
28. Zhang, Y., Parker, W.B., Sorscher, E.J., Ealick, S.E.: PNP Anticancer Gene Therapy. Curr. Top. Med. Chem. **5**, 1259–1274 (2005)
29. Basso, L.A., Santos, D.S., Shi, W., Furneaux, R.H., Tyler, P.C., Schramm, V.L., Blanchard, J.S.: Purine nucleoside phosphorylase from *Mycobacterium tuberculosis.* Analysis of inhibition by a transition-state analogue and dissection by parts. Biochemistry **40**, 8196–8203 (2001)
30. Lewandowicz, A., Schramm, V.L.: Transition state analysis for human and *Plasmodium falciparum* purine nucleoside phosphorylases. Biochemistry **43**, 1458–1468 (2004)
31. Munagala, N., Wang, C.C.: The purine nucleoside phosphorylase from *Trichomonas vaginalis* is a homologue of the bacterial enzyme. Biochemistry **41**, 10382–10389 (2002)
32. Pereira, H.D.M., Franco, G.R., Cleasby, A., Garratt, R.C.: Structures for the potential drug target purine nucleoside phosphorylase from *Schistosoma mansoni* causal agent of schistosomiasis. J. Mol. Biol. **353**, 584–599 (2005)
33. Wales, T.E., Fadgen, K.E., Gerhardt, G.C., Engen, J.R.: High-speed and high-resolution UPLC separation at zero degrees celsius. Anal. Chem. **80**, 6815–6820 (2008)
34. Karplus, M., Kuriyan, J.: Molecular dynamics and protein function. Proc. Natl. Acad. Sci. U. S. A. **102**, 6679–6685 (2005)
35. Best, R.B., Vendruscolo, M.: Structural interpretation of hydrogen exchange protection factors in proteins: characterization of the native state fluctuations of CI2. Structure **14**, 97–106 (2006)
36. Sljoka, A., Wilson, D.: Probing protein ensemble rigidity and hydrogen-deuterium exchange. Phys. Biol. **10**, 1–26 (2013)
37. Hilser, V.J., Freire, E.: Structure-based calculation of the equilibrium folding pathway of proteins. Correlation with hydrogen exchange protection factors. J. Mol. Biol. **262**, 756–772 (1996)
38. Hilser, V., Whitten, S.: Using the COREX/BEST Server to Model the Native-State Ensemble. In: Livesay D.R. (ed.) Protein Dynamics. Springer Science+Business Media, New York Humana Press (2014)
39. Liu, T., Pantazatos, D., Li, S., Hamuro, Y., Hilser, V.J., Woods, V.L.: Quantitative assessment of protein structural models by comparison of H/D exchange MS rata with exchange behavior accurately predicted by DXCOREX. J. Am. Soc. Mass Spectrom. **23**, 43–56 (2012)
40. Petruk, A.A., Defelipe, L.A., Rodríguez Limardo, R.G., Bucci, H., Marti, M.A., Turjanski, A.G.: Molecular dynamics simulations provide atomistic insight into hydrogen exchange mass spectrometry experiments. J. Chem. Theory Comput. **9**, 658–669 (2013)
41. Radou, G., Dreyer, F.N., Tuma, R., Paci, E.: Functional dynamics of hexameric helicase probed by hydrogen exchange and simulation. Biophys. J. **107**, 983–990 (2014)
42. McAllister, R.G., Konermann, L.: Challenges in the interpretation of protein H/D exchange data: a molecular dynamics simulation perspective. Biochemistry **54**, 2683–2692 (2015)
43. Skinner, J.J., Lim, W.K., Bédard, S., Black, B.E., Englander, S.W.: Protein hydrogen exchange: testing current models. Protein Sci. **21**, 987–995 (2012)
44. Skinner, J.J., Lim, W.K., Bédard, S., Black, B.E., Englander, S.W.: Protein dynamics viewed by hydrogen exchange. Protein Sci. **21**, 996–1005 (2012)
45. Bzowska, A., Kulikowska, E., Shugar, D.: Formycins A and B and some analogues: selective inhibitors of bacterial (*Escherichia coli*) purine nucleoside phosphorylase. Biochim. Biophys. Acta **1120**, 239–247 (1992)
46. Shugar, D., Psoda, A.: In: Saenger, W. (ed.) 4.12.2 Predominant Tautomeric Species of Nucleic Acid Components. Springer, Berlin and Heidelberg (1990)
47. Tarnowski, K., Fituch, K., Szczepanowski, R.H., Dadlez, M., Kaus-Drobek, M.: Patterns of structural dynamics in RACK1 protein retained throughout evolution: a hydrogen-deuterium exchange study of three orthologs. Protein Sci. **23**, 639–651 (2014)
48. Kazazic, S., Zhang, H.-M., Schaub, T., Emmett, M., Hendrickson, C., Blakney, G., Marshall, A: Automated data reduction for hydrogen/deuterium exchange experiments, enabled by high-resolution fourier transform ion cyclotron resonance mass spectrometry. J. Am. Soc. Mass Spectrom. **21**, 550–558 (2010)
49. Houde, D., Berkowitz, S.A., Engen, J.R.: The utility of hydrogen/deuterium exchange mass spectrometry in biopharmaceutical comparability studies. J. Pharm. Sci. **100**, 2071–2086 (2011)
50. Mao, C., Cook, W.J., Zhou, M., Koszalka, G.W., Krenitsky, T.A., Ealick, S.E.: The crystal structure of *Escherichia coli* purine nucleoside phosphorylase: a comparison with the human enzyme reveals a conserved topology. Structure **5**, 1373–1383 (1997)
51. Vriend, G.: WHAT IF: A molecular modeling and drug design program. J. Mol. Graph. **8**, 52–56 (1990)
52. Case, D., Darden, T., Cheatham III, T., Simmerling, C., Wang, J., Duke, R., Luo, R., Merz, K., Wang, B.,Pearlman, D.: AMBER 8, 5th edn, p. 39. University of California, San Francisco (2004)
53. Duan, Y., Wu, C., Chowdhury, S., Lee, M.C., Xiong, G., Zhang, W., Yang, R., Cieplak, P., Luo, R., Lee, T., Cladwell, J., Wang, J., Kollman, P.: A point-charge force field for molecular mechanics simulations of proteins based on condensed-phase quantum mechanical calculations. J. Comput. Chem. **24**, 1999 III 2012 (2003)
54. Jorgensen, W.L., Chandrasekhar, J., Madura, J.D., Impey, R.W., Klein, M.L.: Comparison of simple potential functions for simulating liquid water. J. Chem. Phys. **79**, 926–935 (1983)
55. Aaqvist, J.: Ion-water interaction potentials derived from free energy perturbation simulations. J. Phys. Chem. **94**, 8021–8024 (1990)
56. Berendsen, H.J.C., Postma, J.P.M., van Gunsteren, W.F., DiNola, A., Haak, J.R.: Molecular dynamics with coupling to an external bath. J. Chem. Phys. **81**, 3684–3690 (1984)
57. Hess, B., Kutzner, C., van der Spoel, D., Lindahl, E.: GROMACS 4: algorithms for highly efficient, load-balanced, and scalable molecular simulation. J. Chem. Theory Comput. **4**, 435–447 (2008)
58. Humphrey, W., Dalke, A., Schulten, K.: VMD—Visual Molecular Dynamics. J. Mol. Graph **14**, 33–38 (1996)
59. Spence, J.: X-ray lasers and serial crystallography. IUCrJ. **2**, 305–306 (2015)